The Astrophysical Journal, 989:36 (7pp), 2025 August 10 https://doi.org/10.3847/1538-4357/adef0c

Radio Morphology of Gamma-Ray Sources. II. Giant Radio Galaxies

Vaidehi S. Paliya[1], D. J. Saikia[1], G. Bruni[2], Alberto Domínguez[3], and C. S. Stalin[4]
[1] Inter-University Centre for Astronomy and Astrophysics (IUCAA), SPPU Campus, Pune 411007, India; vaidehi.s.paliya@gmail.com
[2] INAF – Istituto di Astrofisica e Planetologia Spaziali, Via Fosso del Cavaliere 100, 00133 Rome, Italy
[3] IPARCOS and Department of EMFTEL, Universidad Complutense de Madrid, E-28040 Madrid, Spain
[4] Indian Institute of Astrophysics, Block II, Koramangala, Bengaluru 560034, Karnataka, India
Received 2025 April 23; revised 2025 June 27; accepted 2025 July 3; published 2025 August 1

Abstract

Giant radio sources, including galaxies and quasars (hereafter GRSs), are active galactic nuclei (AGN) hosting relativistic jets with source sizes exceeding a projected length of 0.7 Mpc. They are crucial to understanding the evolution of radio sources and their interaction with the surrounding environment. Some of these enigmatic objects, e.g., NGC 315, have also been reported as γ-ray emitters. Since GRSs are thought to be aligned close to the plane of the sky, they are invaluable targets to explore the radiative mechanisms responsible for the observed γ-ray emission. We have carried out a systematic search of γ-ray-emitting GRSs using sensitive low-resolution radio surveys, such as by the Low Frequency Array, NRAO Very Large Array Sky Survey, and Rapid ASKAP Continuum Survey, and considering the fourth data release of the fourth Fermi Large Area Telescope γ-ray source (4FGL-DR4) catalog. By carefully inspecting the radio maps of all AGN included in the 4FGL-DR4 catalog, we have identified 16 γ-ray-emitting GRSs, including eight that are being reported as GRSs for the first time. Some of their observed parameters, e.g., core dominance, appeared to differ from those found for the non-γ-ray detected GRS population, possibly due to the relatively small viewing angle of the γ-ray-emitting jet. The observed γ-ray properties of these objects were found to be similar to those of non-GRS γ-ray-emitting misaligned AGN. We conclude that the origin of the γ-ray emission could be similar in both source populations.

Unified Astronomy Thesaurus concepts: Gamma-ray astronomy (628); Giant radio galaxies (654)

1. Introduction

Relativistic jets manifest some of the most intriguing processes involving the interaction of matter and energy at the centers of galaxies. The projected lengths of the sources fed by these jets range from a few parsecs (pc), for compact symmetric objects, to ∼Mpc scales for giant radio sources (e.g., A. G. Willis et al. 1974; P. N. Wilkinson et al. 1994; M. S. S. L. Oei et al. 2024). Active galactic nuclei (AGN) hosting powerful relativistic jets are often termed radio-loud AGN. They have been classified as Fanaroff–Riley type I (FR I) and type II (FR II) radio sources based on their radio power, with the latter being the more luminous ones (B. L. Fanaroff & J. M. Riley 1974). Originally, radio sources were classified in this scheme based on their distinct radio morphologies, with FR I sources exhibiting edge-darkened, diffuse radio structures. The FR II sources, on the other hand, showed large-scale, edge-brightened radio lobes with bright hotspots. However, recent Low Frequency Array (LOFAR) observations have revealed several outliers, e.g., low-power FR II sources and vice versa (B. Mingo et al. 2019). The radio-loud AGN have also been classified as low-excitation radio galaxies (LERGs) and high-excitation radio galaxies (HERGs) based on the accretion activity. The HERGs exhibit radiatively efficient accretion ($L_{\rm bol.}/L_{\rm Edd} > 0.01$; e.g., P. N. Best & T. M. Heckman 2012). The relationship between the FR class and mode of accretion, i.e., radiatively efficient/inefficient, is complex, with no clear pattern emerging from observations (B. Mingo et al. 2019, 2022).

Among the jetted AGN population, giant radio sources, associated both with radio galaxies and quasars (hereafter GRSs), are one of the most intriguing members, exhibiting gigantic source sizes produced by the relativistic jets (projected length $\gtrsim$0.7 Mpc; A. G. Willis et al. 1974). For example, recent LOFAR observations have revealed the source Porphyrion hosting a jet exceeding 7 Mpc (M. S. S. L. Oei et al. 2024). The largest catalog of GRSs has recently been published by R. I. J. Mostert et al. (2024), reporting more than 11,000 sources (see also P. Dabhade et al. 2023 for a review). A majority of GRSs are reported to be of FR II type, and only a minor fraction have been identified as FR I (see C. H. Ishwara-Chandra & D. J. Saikia 1999; A. Kuźmicz et al. 2018; P. Dabhade et al. 2020a, 2020b). Some GRSs also exhibit signatures of episodic jet activity (e.g., A. P. Schoenmakers et al. 2000; A. Kuźmicz et al. 2017; V. H. Mahatma et al. 2019; K. Chavan et al. 2023; P. Dabhade et al. 2024). These objects are usually powered by massive black holes ($>10^8 M_\odot$) similar to other non-GRS radio galaxies and quasars (see A. Kuźmicz & M. Jamrozy 2012; P. Dabhade et al. 2020b). A major fraction of these objects exhibit an LERG-type accretion activity (A. Kuźmicz & M. Jamrozy 2012).

F. Ursini et al. (2018) carried out a broadband X-ray spectral analysis of a sample of hard X-ray selected GRSs and reported the X-ray emission to originate from the X-ray corona illuminated by radiatively efficient accretion. The nuclear X-ray emission was more luminous than the jet power and radio lobe luminosity, indicating a restarted AGN activity. Subsequent high-resolution radio observations have revealed the presence of young radio sources in the cores of hard X-ray selected GRSs, thus indicating possible rejuvenated AGN activity episode (G. Bruni et al. 2019, 2020).

The deepest survey of the γ-ray sky is being conducted by the Fermi Large Area Telescope (LAT; W. B. Atwood et al. 2009). In its first 14 yr of operation, summarized in the fourth data release of the fourth Fermi-LAT γ-ray source catalog (4FGL-DR4), Fermi-LAT has detected 7194 γ-ray sources in the 50 MeV–1 TeV range (S. Abdollahi et al. 2022; J. Ballet et al. 2023), the majority of which are blazars, i.e., AGN with jets directed close to our line of sight. In contrast, only a small number of misaligned AGN ($\sim$50) were reported, and they have been found to be contributing up to $\sim$10% of the extragalactic γ-ray background (Y. Fukazawa et al. 2022). The 4FGL-DR4 catalog also reported 1624 blazar candidates of uncertain type, i.e., sources whose multiwavelength behavior is similar to blazars though they lack optical spectroscopic classification (M. Ackermann et al. 2011; S. Abdollahi et al. 2022). All in all, there are 4069 γ-ray-emitting AGN present in the 4FGL-DR4 catalog. Furthermore, the γ-ray emission from misaligned AGN has been explained with the synchrotron self-Compton process along with more complex models, such as spine-sheath structured jets (D. Giannios et al. 2010; G. Migliori et al. 2011; Y. Fukazawa et al. 2018).

The properties of GRSs in the γ-ray band are not well explored. Only a few objects of this class have been studied, as members of the general γ-ray detected misaligned jetted AGN population (Y. Fukazawa et al. 2022). Considering the AGN unification, GRSs are seen at large viewing angles. Indeed, the core dominance fraction, an indicator of the jet viewing angle, was found to decrease with increasing projected jet length (e.g., V. K. Kapahi & D. J. Saikia 1982). The GRSs also have smaller core dominance compared to non-GRS radio sources (see M. Mahato et al. 2022). This observation can explain the paucity of γ-ray detected GRSs in the γ-ray source catalogs, since γ-ray emission is highly sensitive to the viewing angle (e.g., C. D. Dermer 1995). Interestingly, Y.-W. Yu et al. (2024) reported the detection of γ-ray emission from the radio lobes of a GRS, NGC 6251 ($z = 0.02$), indicating a different γ-ray-emitting region location or physical mechanism compared to that usually considered for the beamed AGN or blazar population (see V. S. Paliya et al. 2017).

In V. S. Paliya et al. (2024, hereafter Paper I), we started a program to identify the γ-ray-emitting misaligned jetted AGN population by utilizing the sensitive radio data provided by ongoing surveys, e.g., LOFAR. We used small beam size survey data, e.g., the Very Large Array Sky Survey (VLASS), to identify radio sources that might have remained unresolved in earlier surveys and found 149 double-lobed objects exhibiting multiwavelength behavior, e.g., radio spectrum and optical spectroscopic properties, similar to misaligned AGN (see also A. A. Abdo et al. 2010; G. Chiaro et al. 2020). However, a drawback of choosing high-resolution data is that some misaligned sources with large-scale diffuse radio emissions, such as GRSs, may have been missed. Therefore, in this work, we adopted radio surveys with the lowest resolution, thus the largest restoring beams, to identify potential γ-ray-emitting GRSs and improve the completeness of the γ-ray detected misaligned AGN population. Section 2 briefly describes the sample selection and radio surveys whose data were adopted in this work. We present our findings in Section 3 and discuss them in Section 4. We summarize the results in Section 5. Throughout, we have adopted the flux density $F_\nu \propto \nu^\alpha$, where α is the radio spectral index. A flat cosmology with $H_0 = 70\,\mathrm{km\,s^{-1}\,Mpc^{-1}}$ and $\Omega_M = 0.3$ was used.

2. Sample Selection and Multiwavelength Catalog

2.1. The Sample

We used the 4FGL-DR4 catalog, which lists 7194 γ-ray sources (S. Abdollahi et al. 2022; J. Ballet et al. 2023). From this sample, we considered 4069 objects whose multiwavelength counterparts have been reported to be AGN.

2.2. Radio Catalogs

LOFAR Two-meter Sky Survey. The second data release of the LOFAR Two-meter Sky Survey provides the cutout images at 144 MHz with resolutions of 6″ and 20″ (T. W. Shimwell et al. 2022). Since our primary objective was to identify the large-scale diffuse radio emission, we downloaded $30' \times 30'$ cutout images of 935 objects that have a resolution of 20″.[5]

NRAO-VLA Sky Survey (NVSS). This is a 1.4 GHz continuum survey covering the sky north of $-40°$ decl.. The resolution of the survey is 45″ and the rms brightness fluctuations are about 0.45 mJy beam^{-1} (see J. J. Condon et al. 1998 for details). We downloaded 1×1 deg^2 cutout images of 4531 sources from the SkyView Virtual Observatory website.[6]

Rapid ASKAP Continuum Survey (RACS). This first data release of this survey covered the whole sky between decl. $-80°$ and $+30°$ at an operating frequency of 888 MHz and a resolution of 25″ (C. L. Hale et al. 2021). We considered the $30' \times 30'$ cutout images of 2337 objects and downloaded them from the CSIRO ASKAP science data archive.[7]

3. Results

We visually examined the radio morphology of all γ-ray sources and retained those with projected largest angular size (LAS) $\gtrsim 1'$. This is because at redshifts 0.1, 0.5, and 1, a linear size of 700 kpc corresponds to $6'.3$, $1'.9$, and $1'.4$, respectively. Therefore, any radio source with an LAS exceeding $1'$ will likely be a GRS candidate. We followed a strategy to compute the parameters similar to that adopted in our previous work (Paper I). In particular, to derive the LAS, we used the survey data in which the source is best resolved. The LAS was measured from the 3σ outermost flux density contour level for FR I morphologies. For FR II sources, on the other hand, it was estimated from the brightest pixel on the hotspot. To determine the 3σ contour levels, the rms noise value (σ) was computed from a nearby region free from the source contamination. Finally, only sources with available spectroscopic/photometric redshifts were considered to convert the measured LAS to physical units in kiloparsecs. This exercise led to a final sample of 16 γ-ray-emitting GRSs. Table 1 provides the basic information about these sources, and we show their radio maps in Figure 1.

We also derived the core dominance, which is considered a good proxy for the orientation of the beamed emission since the lobe emission is isotropic, whereas the core emission is Doppler boosted (e.g., R. Morganti et al. 1997). The following

[5] https://lofar-surveys.org/dr2_release.html
[6] https://skyview.gsfc.nasa.gov/current/cgi/query.pl
[7] https://research.csiro.au/casda/

Table 1
The List of γ-ray-emitting Misaligned Jetted AGN Hosting Mpc-scale Radio Sources

4FGL Name	Other Name	z	LAS (Mpc)	$F_{\rm core}$ (mJy)	$F_{\rm total}$ (mJy)	α	$C_{\rm r}D$	Survey	Morph.	References
(1)	(2)	(3)	(4)	(5)	(6)	(7)	(8)	(9)	(10)	(11)
J0037.9+2612	GB6 B0034+2556	0.148	410 (1.07)	80	550	−0.37	0.32	L, V, L	FR I	A20
J0049.0+2252	PKS J0049+2253	0.264	220 (0.89)	141	1660	−0.51	0.10	L, V, L	FR I	A20
J0057.7+3023	NGC 315	0.017	5300 (1.84)	500	13400	−0.30	−0.35	L, V, L	FR I-II	J00
J0126.5−1553	PMN J0127−1556	0.988	94 (0.76)	25	150	−0.55	−0.03	R, V, R	FR II	F22
J0312.9+4119	B3 0309+411B	0.134	530 (1.27)	310	520	−0.01	0.49	N, V, N	FR I	K22
J0525.6−2008	PMN J0525−2010	0.092	700 (1.20)	110	455	−0.19	−0.04	R, V, R	FR I	P21
J0617.7−1715	IVS B0615−172	0.098	650 (1.18)	150	805	−0.22	−0.33	N, V, N	FR I	S13
J0946.0+4735	RX J0946.0+4735	0.569	210 (1.41)	15	66	−0.32	0.71	L, V, L	FR I	A20
J1202.4+4442	GB6 J1202+4444	0.297	180 (0.79)	45	390	−0.46	0.27	L, V, L	FR I	A20
J1226.9+6405	GB6 J1226+6406	0.110	425 (0.86)	40	650	−0.18	−0.06	L, V, L	FR I-II	A20
J1230.9+3711	GB6 J1231+3711	0.218	255 (0.91)	17	190	−0.74	−0.67	N, V, N	FR I	A20
J1630.6+8234	NGC 6251	0.020	3400 (1.38)	510	2150	−0.05	−0.23	N, V, N	FR I-II	W03
J2228.5+2211	GB6 B2226+2156	0.710	190 (1.39)	30	120	−0.27	0.78	L, V, L	FR I	A20
J2253.3+3233	TXS 2250+323	0.258	250 (1.00)	125	340	−0.05	0.89	L, V, L	FR I	T17
J2302.8−1841	PKS 2300−18	0.128	325 (0.75)	235	1981	−0.55	−0.41	R, V, R	FR I	J09
J2333.9−2343	PKS 2331−240	0.047	1130 (1.05)	970	1150	0.13	1.01	N, V, N	FR II	K22

Note. The column details are as follows: (1) 4FGL name; (2) counterpart name; (3) redshift; (4) largest angular size (and the corresponding linear size) in arcseconds; (5) and (6) core and total flux densities, respectively; (7) radio spectral index provided in SPECFIND; (8) core dominance; (9) the surveys that were used to estimate the LAS, core, and total flux densities, in respective order, where V = VLASS, L = LOFAR, N = NVSS, and R = RACS; and (10) morphological classification. In the first column, source names written in boldface are reported as GRSs for the first time in this work. The last column provides the references of the optical spectra and redshift: A20: R. Ahumada et al. (2020), J00: R. A. Jansen et al. (2000), F22: L. Foschini et al. (2022), K22: M. J. Koss et al. (2022), P21: S. Paiano et al. (2021), S13: M. S. Shaw et al. (2013), W03: G. Wegner et al. (2003), T17: O. Titov et al. (2017), and J09: D. H. Jones et al. (2009).

relation was adopted:

$$C_{\rm r}D = \log\left(\frac{F_{\rm core}}{F_{\rm ext}}(1+z)^{\alpha_{\rm core}-\alpha_{\rm ext}}\right). \quad (1)$$

The parameters $\alpha_{\rm ext}$ and $\alpha_{\rm core}$ are spectral indices ($F(\nu) \propto \nu^{\alpha}$) of the extended and core emission, respectively, and were taken as $\alpha_{\rm ext} = -0.8$ and $\alpha_{\rm core} = 0$. The core and extended flux densities, $F_{\rm core}$ and $F_{\rm ext}$ ($=F_{\rm total} - F_{\rm core}$), were calculated at rest-frame 3 GHz assuming the spectral indices mentioned above. We derived $F_{\rm total}$ using the survey data with the largest restoring beam to consider all the diffuse extended flux. To estimate $F_{\rm core}$, we used the high-resolution VLASS data, which allowed us to distinguish the core component from extended lobes properly. Typical uncertainties in the flux densities, including calibration errors, are about 10% (see, e.g., C. L. Hale et al. 2021; T. W. Shimwell et al. 2022). Furthermore, we collected the overall radio spectral indices for all sources using the SPECFIND (v3.0) catalog (Y. Stein et al. 2021). The core dominance and radio spectral indices along with $F_{\rm core}$ and $F_{\rm total}$ values are provided in Table 1.

Spectroscopic redshifts are available in the literature for all sources except 4FGL J0126.5−1553 or PMN J0127−1556. We adopted the photometric redshift of $z = 0.988$ for this object from L. Foschini et al. (2022). The optical spectra of four objects, 4FGL J0312.9+4119, 4FGL J2302.8−1841, 4FGL J2253.3+3233, and 4FGL J2333.9−2343, show broad emission lines suggesting they are powered by radiatively efficient accretion processes (see references in Table 1). For the remaining 11 sources, absorption features from the host galaxy stellar population dominate their optical spectra. The lack of strong emission lines suggests they are likely LERG-type objects.

4. Discussion

Identifying GRSs in the high-energy γ-ray band is important since they are thought to lie close to the plane of the sky. Hence, the observed radiation is not expected to be significantly Doppler boosted. Therefore, these objects can be promising candidates to explore the origin of the γ-ray emission. We utilized the data from the sensitive, low-resolution surveys, LOFAR, NVSS, and RACS, and carefully inspected the morphologies of all γ-ray sources. This exercise identified 16 objects with projected source sizes exceeding 0.7 Mpc. Among them, eight are reported as GRSs for the first time in this work. These objects are highlighted in boldface in Table 1. The identification of such a large number of γ-ray-emitting GRSs demonstrates the capabilities of the latest surveys in revealing the intriguing faint extended emission associated with relativistic jets.

These surveys have also revealed a complex morphology of several of the γ-ray-emitting GRSs (Figure 1). Some of them, e.g., 4FGL J0525.6−2008, exhibit bent radio jets resembling wide-angled tailed sources. Interestingly, $\gtrsim$50% of the sources show diffuse, low-surface brightness extended radio emission, sometimes on one side of the source, similar to FR I sources. This finding is in contrast with the general non-γ-ray detected GRS population, where the known samples are reported to be dominated by FR II radio sources (see C. H. Ishwara-Chandra & D. J. Saikia 1999; A. Kuźmicz et al. 2018; P. Dabhade et al. 2020a, 2020b).

GRSs usually show a steep radio spectrum ($\alpha \sim -0.75$; P. Dabhade et al. 2020a, 2020b). Interestingly, most of the γ-ray-emitting GRSs exhibit a flat or inverted radio spectrum ($\alpha \gtrsim -0.5$). The radio spectral index was found to be <-0.5 only for four sources (Table 1). Since these objects are γ-ray emitters, they might be viewed at a relatively small viewing

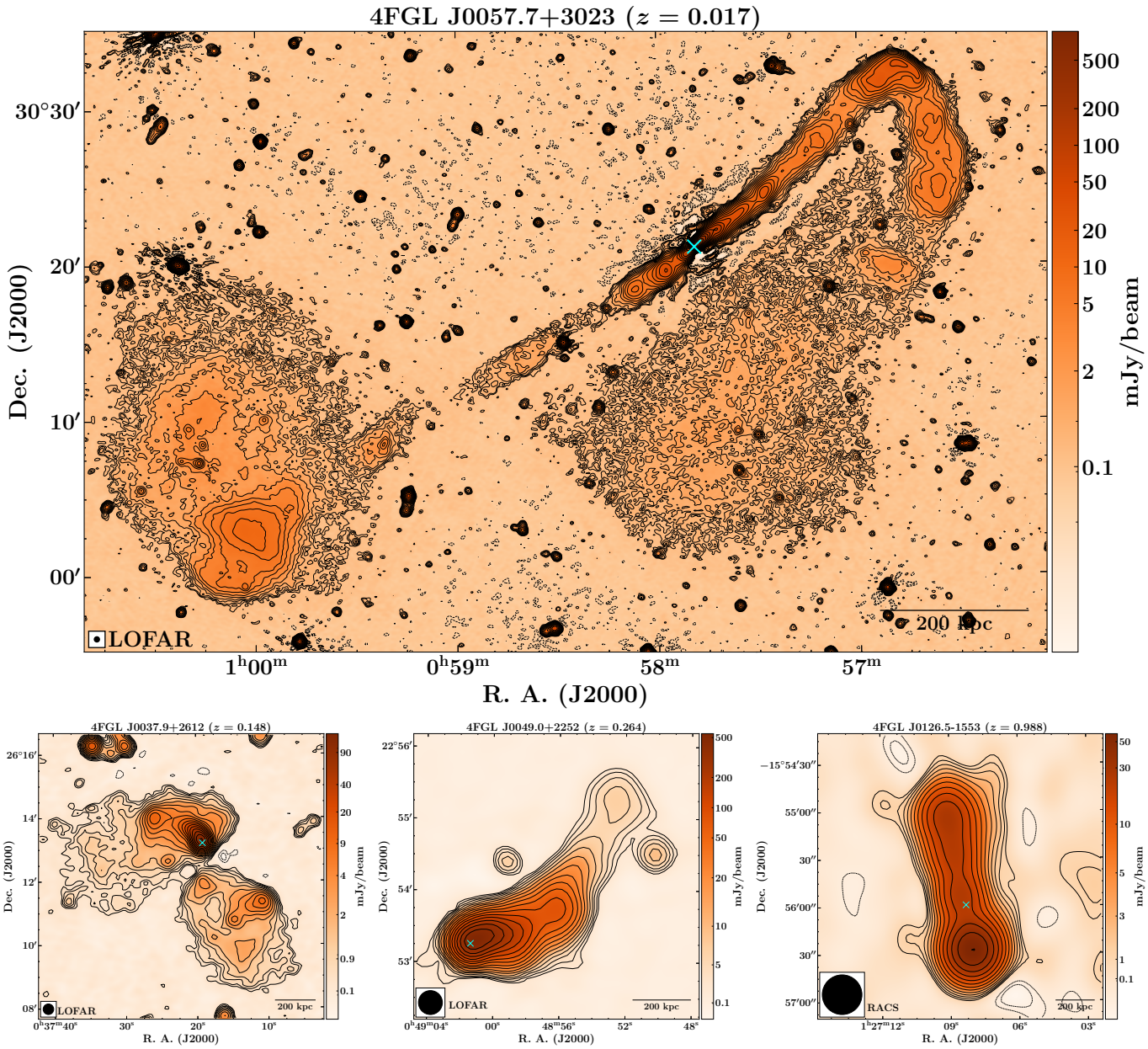

Figure 1. The radio morphologies of γ-ray detected GRSs. In all plots, the contour levels start at 3 × rms × $(-2, -\sqrt{2}, -1, 1)$ and increase in multiples of $\sqrt{2}$. The beam size and the name of the considered survey are shown in the bottom-left corner. The north is up and east to the left. The crosses mark the positions of the optical objects.

angle compared to the general, non-γ-ray detected GRS population, leading to the observation of a flatter radio spectrum.

The core dominance is found to be small (<1) for γ-ray detected radio galaxies (R. Angioni et al. 2019; Paper I). On the other hand, blazars exhibit a core-dominated radio emission ($C_rD > 1$; M. J. Marchã et al. 2001; Y. Y. Chen et al. 2015). For four sources, we found $C_rD > 0.5$, indicating a possible beamed core emission. Indeed, one of them, 4FGL J2333.9−2343 or PKS 2331−240, has been reported to host a blazar nucleus, suggesting a possible jet bending with the inner jet aligned toward us (L. Hernández-García et al. 2017, 2023). Another source, 4FGL J0946.0+4735 or RX J0946.0+4735, was earlier classified as a BL Lac object. Moreover, there are four γ-ray-emitting GRSs with $C_rD > 0$ (on log scale), indicating a nonnegligible core contribution. This finding is consistent with the relatively flat radio spectrum observed from some of these objects. The lobe emission was found to be dominating over the core for the remaining GRSs, suggesting a larger viewing angle of the jet. The observed γ-ray emission from these objects could have significant contribution from the lobes similar to that observed from Cen A and NGC 6251 (see F. Aharonian et al. 2009; M. Persic & Y. Rephaeli 2019; Y.-W. Yu et al. 2024).

In the left panel of Figure 2, we show the distribution of the γ-ray photon index with the γ-ray luminosity for Fermi-LAT detected AGN. As can be seen, the distribution of the γ-ray detected GRSs is similar to that of the non-GRS misaligned AGN population (see also G. Bruni et al. 2022; Paper I). This result hints at the similar radiative processes working for both

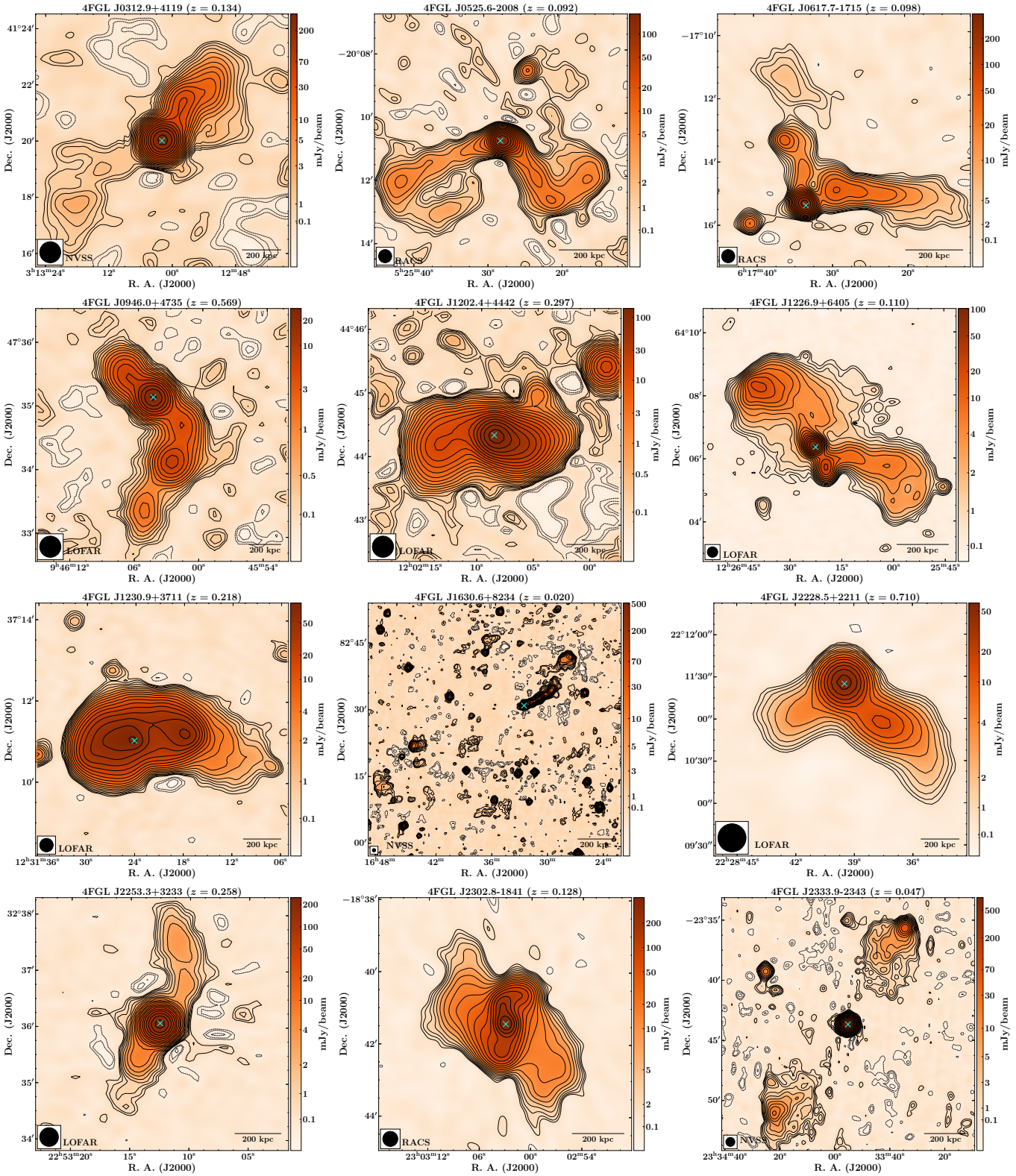

Figure 1. (Continued.)

source populations and radiating the γ-ray emission. Furthermore, most GRSs have soft γ-ray spectra (photon index >2), indicating the high-energy radiation to be produced by the tail end of the electron population. This is because the γ-ray softening due to extragalactic background light attenuation may not be important since all sources are located in the nearby Universe ($z < 1$; see A. Domínguez & M. Ajello 2015). Since most of the sources have only a weak accretion activity, as revealed by the lack of strong optical emission lines, the γ-ray absorption due to pair production with the broad-line region photon field is also not expected to be crucial (see M. Böttcher & P. Els 2016). A detailed multiwavelength study

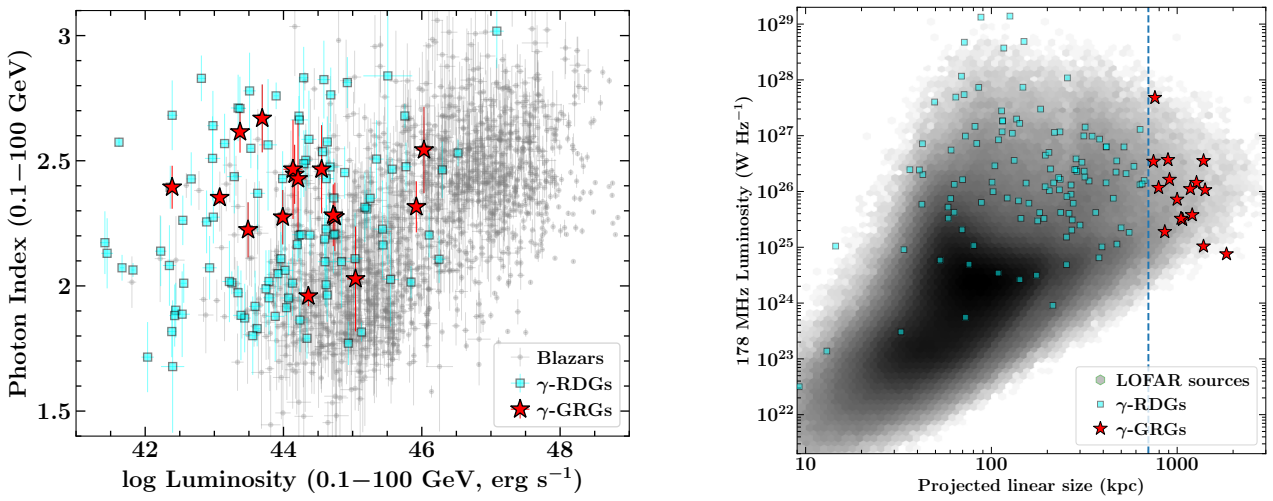

(a) (b)

Figure 2. Left: the γ-ray luminosity vs. photon index plane for γ-ray-emitting jetted sources. For a comparison, we also show blazars with gray circles. Right: this plot shows the variation of 178 MHz radio power with the projected linear size. The gray data points belong to LOFAR-detected AGN. The vertical dashed line shows the boundary line (700 kpc) for a source to be termed as a GRS. In both panels, the red stars represent the γ-ray detected GRSs and the cyan squares refer to the general γ-ray-emitting misaligned AGN population.

of these objects may provide clues about the origin of the γ-ray emission.

We used the LOFAR results to plot the power/linear-size ($P - D$) diagram and examine the location of γ-ray-emitting GRSs in it (Figure 2, right panel; e.g., J. E. Baldwin 1982; C. R. Kaiser et al. 1997; M. J. Hardcastle et al. 2019, 2023). Assuming a spectral slope of -0.8, we extrapolated the observed total flux densities of the γ-ray-emitting misaligned AGN, including GRSs, to that at 178 MHz in the rest frame. The distribution of the γ-ray-detected objects was similar to that of the general LOFAR-detected AGN population.

5. Summary

We have utilized the high-quality, low-resolution radio survey data sets to search for GRSs in the sample of astrophysical objects detected with the Fermi-LAT. We summarize our results as follows:

1. We report the identification of 16 GRSs among the γ-ray sources included in the 4FGL-DR4 catalog, including eight identified as GRSs for the first time.
2. Several γ-ray-detected GRSs exhibit complex radio morphologies, though a significant fraction ($\gtrsim$50%) show low-surface-brightness features characteristic of FR I radio sources. This finding is in tension with non-γ-ray-emitting GRSs, which have been reported to be dominated by FR II-shaped morphologies.
3. We derived the core dominance at rest-frame 3 GHz and found several objects to have core-dominated emission ($C_{\rm r}D > 0$, on log scale). On the other hand, the non-γ-ray-detected GRSs usually have lobe-dominated emission, as reported in earlier studies. The differences could be because the γ-ray detection indicates a relatively small viewing angle of the jet, which can explain their significant core dominance.
4. In the γ-ray luminosity versus γ-ray photon index plane and P–D diagram, γ-ray detected GRSs tend to occupy the same region as non-GRS γ-ray-emitting misaligned AGN. These results hint that the origin of the γ-ray emission could be the same in both source populations.

Acknowledgments

We thank the journal referee for constructive criticism. A.D. is thankful for the support of the Proyecto PID2021-126536OA-I00 funded by MCIN/AEI/10.13039/501100011033. G.B. acknowledges financial support for the GRACE project, selected through the Open Space Innovation Platform (https://ideas.esa.int) as a Co-Sponsored Research Agreement and carried out under the Discovery program of and funded by the European Space Agency (agreement No. 4000142106/23/NL/MGu/my). G.B. acknowledges financial support from the Bando Ricerca Fondamentale INAF 2023 for the project "The GRACE project: high-energy giant radio galaxies and their duty cycle."

The National Radio Astronomy Observatory is a facility of the National Science Foundation operated under cooperative agreement by Associated Universities, Inc.

LOFAR is the Low Frequency Array designed and constructed by ASTRON. It has observing, data processing, and data storage facilities in several countries, which are owned by various parties (each with their own funding sources), and which are collectively operated by the ILT foundation under a joint scientific policy. The ILT resources have benefited from the following recent major funding sources: CNRS-INSU, Observatoire de Paris and Université d'Orléans, France; BMBF, MIWF-NRW, MPG, Germany; Science Foundation Ireland (SFI), Department of Business, Enterprise and Innovation (DBEI), Ireland; NWO, the Netherlands; the Science and Technology Facilities Council, UK; Ministry of Science and Higher Education, Poland; and the Istituto Nazionale di Astrofisica (INAF), Italy.

This paper includes archived data obtained through the CSIRO ASKAP Science Data Archive, CASDA (https://data.csiro.au). This research uses services or data provided by the Astro Data Lab, which is part of the Community Science and Data Center (CSDC) Program of NSF NOIRLab.

ORCID iDs

Vaidehi S. Paliya https://orcid.org/0000-0001-7774-5308
D. J. Saikia https://orcid.org/0000-0002-4464-8023
G. Bruni https://orcid.org/0000-0002-5182-6289
Alberto Domínguez https://orcid.org/0000-0002-3433-4610
C. S. Stalin https://orcid.org/0000-0002-4998-1861

References

Abdo, A. A., Ackermann, M., Ajello, M., et al. 2010, ApJ, 720, 912
Abdollahi, S., Acero, F., Baldini, L., et al. 2022, ApJS, 260, 53
Ackermann, M., Ajello, M., Allafort, A., et al. 2011, ApJ, 743, 171
Aharonian, F., Akhperjanian, A. G., Anton, G., et al. 2009, ApJL, 695, L40
Ahumada, R., Allende Prieto, C., Almeida, A., et al. 2020, ApJS, 249, 3
Angioni, R., Ros, E., Kadler, M., et al. 2019, A&A, 627, A148
Atwood, W. B., Abdo, A. A., Ackermann, M., et al. 2009, ApJ, 697, 1071
Baldwin, J. E. 1982, in IAU Symp. 97, Extragalactic Radio Sources, ed. D. S. Heeschen & C. M. Wade (Cambridge: Cambridge Univ. Press), 21
Ballet, J., Bruel, P., Burnett, T. H., Lott, B. & The Fermi-LAT Collaboration 2023, arXiv:2307.12546
Best, P. N., & Heckman, T. M. 2012, MNRAS, 421, 1569
Böttcher, M., & Els, P. 2016, ApJ, 821, 102
Bruni, G., Bassani, L., Persic, M., et al. 2022, MNRAS, 513, 886
Bruni, G., Panessa, F., Bassani, L., et al. 2019, ApJ, 875, 88
Bruni, G., Panessa, F., Bassani, L., et al. 2020, MNRAS, 494, 902
Chavan, K., Dabhade, P., & Saikia, D. J. 2023, MNRAS, 525, L87
Chen, Y. Y., Zhang, X., Zhang, H. J., & Yu, X. L. 2015, MNRAS, 451, 4193
Chiaro, G., La Mura, G., Domínguez, A., & Bisogni, S. 2020, JHEAp, 27, 77
Condon, J. J., Cotton, W. D., Greisen, E. W., et al. 1998, AJ, 115, 1693
Dabhade, P., Chavan, K., Saikia, D. J., Oei, M. S. S. L., & Rottgering, H. J. A. 2024, A&A, 696, A97
Dabhade, P., Mahato, M., Bagchi, J., et al. 2020b, A&A, 642, A153
Dabhade, P., Röttgering, H. J. A., Bagchi, J., et al. 2020a, A&A, 635, A5
Dabhade, P., Saikia, D. J., & Mahato, M. 2023, JApA, 44, 13
Dermer, C. D. 1995, ApJL, 446, L63
Domínguez, A., & Ajello, M. 2015, ApJL, 813, L34
Fanaroff, B. L., & Riley, J. M. 1974, MNRAS, 167, 31P
Foschini, L., Lister, M. L., Andernach, H., et al. 2022, Univ, 8, 587
Fukazawa, Y., Matake, H., Kayanoki, T., Inoue, Y., & Finke, J. 2022, ApJ, 931, 138
Fukazawa, Y., Shiki, K., Tanaka, Y., et al. 2018, ApJ, 855, 93
Giannios, D., Uzdensky, D. A., & Begelman, M. C. 2010, MNRAS, 402, 1649
Hale, C. L., McConnell, D., Thomson, A. J. M., et al. 2021, PASA, 38, e058
Hardcastle, M. J., Horton, M. A., Williams, W. L., et al. 2023, A&A, 678, A151
Hardcastle, M. J., Williams, W. L., Best, P. N., et al. 2019, A&A, 622, A12
Hernández-García, L., Panessa, F., Bruni, G., et al. 2023, MNRAS, 525, 2187
Hernández-García, L., Panessa, F., Giroletti, M., et al. 2017, A&A, 603, A131
Ishwara-Chandra, C. H., & Saikia, D. J. 1999, MNRAS, 309, 100
Jansen, R. A., Fabricant, D., Franx, M., & Caldwell, N. 2000, ApJS, 126, 331
Jones, D. H., Read, M. A., Saunders, W., et al. 2009, MNRAS, 399, 683
Kaiser, C. R., Dennett-Thorpe, J., & Alexander, P. 1997, MNRAS, 292, 723
Kapahi, V. K., & Saikia, D. J. 1982, JApA, 3, 465
Koss, M. J., Ricci, C., Trakhtenbrot, B., et al. 2022, ApJS, 261, 2
Kuźmicz, A., & Jamrozy, M. 2012, MNRAS, 426, 851
Kuźmicz, A., Jamrozy, M., Bronarska, K., Janda-Boczar, K., & Saikia, D. J. 2018, ApJS, 238, 9
Kuźmicz, A., Jamrozy, M., Kozieł-Wierzbowska, D., & Weżgowiec, M. 2017, MNRAS, 471, 3806
Mahatma, V. H., Hardcastle, M. J., Williams, W. L., et al. 2019, A&A, 622, A13
Mahato, M., Dabhade, P., Saikia, D. J., et al. 2022, A&A, 660, A59
Marchã, M. J., Caccianiga, A., Browne, I. W. A., & Jackson, N. 2001, MNRAS, 326, 1455
Migliori, G., Grandi, P., Torresi, E., et al. 2011, A&A, 533, A72
Mingo, B., Croston, J. H., Best, P. N., et al. 2022, MNRAS, 511, 3250
Mingo, B., Croston, J. H., Hardcastle, M. J., et al. 2019, MNRAS, 488, 2701
Morganti, R., Oosterloo, T. A., Reynolds, J. E., Tadhunter, C. N., & Migenes, V. 1997, MNRAS, 284, 541
Mostert, R. I. J., Oei, M. S. S. L., Barkus, B., et al. 2024, A&A, 691, A185
Oei, M. S. S. L., Hardcastle, M. J., Timmerman, R., et al. 2024, Natur, 633, 537
Paiano, S., Falomo, R., Treves, A., et al. 2021, MNRAS, 504, 3338
Paliya, V. S., Marcotulli, L., Ajello, M., et al. 2017, ApJ, 851, 33
Paliya, V. S., Saikia, D. J., Domínguez, A., & Stalin, C. S. 2024, ApJ, 976, 120
Persic, M., & Rephaeli, Y. 2019, MNRAS, 490, 1489
Schoenmakers, A. P., de Bruyn, A. G., Röttgering, H. J. A., van der Laan, H., & Kaiser, C. R. 2000, MNRAS, 315, 371
Shaw, M. S., Filippenko, A. V., Romani, R. W., Cenko, S. B., & Li, W. 2013, AJ, 146, 127
Shimwell, T. W., Hardcastle, M. J., Tasse, C., et al. 2022, A&A, 659, A1
Stein, Y., Vollmer, B., Boch, T., et al. 2021, A&A, 655, A17
Titov, O., Pursimo, T., Johnston, H. M., et al. 2017, AJ, 153, 157
Ursini, F., Bassani, L., Panessa, F., et al. 2018, MNRAS, 481, 4250
Wegner, G., Bernardi, M., Willmer, C. N. A., et al. 2003, AJ, 126, 2268
Wilkinson, P. N., Polatidis, A. G., Readhead, A. C. S., Xu, W., & Pearson, T. J. 1994, ApJL, 432, L87
Willis, A. G., Strom, R. G., & Wilson, A. S. 1974, Natur, 250, 625
Yu, Y.-W., Zhang, H.-M., Gan, Y.-Y., et al. 2024, ApJ, 965, 163